Digital Discovery

ROYAL SOCIETY OF CHEMISTRY

PAPER

View Article Online
View Journal | View Issue

Cite this: *Digital Discovery*, 2025, **4**, 1276

High-throughput robotic colourimetric titrations using computer vision†

Yuan Li,‡ Biplab Dutta,‡ Qi Jie Yeow, Rob Clowes, Charlotte E. Boott * and Andrew I. Cooper *

A high-throughput (HTE) robotic colourimetric titration workstation was developed using a commercial liquid handling robot (Opentrons OT-2) and computer vision-based analysis. While designed for multiple titration applications, hydrogen peroxide (H_2O_2) determination serves as the most elaborate and well-characterized demonstration of its capabilities. Specifically, potassium permanganate ($KMnO_4$) redox titration was employed to quantify the hydrogen peroxide (H_2O_2) concentration, leveraging the distinct colourimetric transition from colourless to pale pink at the titration endpoint. To monitor this colour change, a webcam was installed on the OT-2 pipette mount, capturing real-time titration progress. Image analysis was enhanced through VGG-augmented UNet for segmentation and the CIELab colour model, ensuring robust and reproducible detection of subtle colour changes. The sensitivity test of the computer vision-aided colour analysis was strongly correlated to UV-vis spectroscopy ($R^2 = 0.9996$), with a good linear dynamic range at low concentrations. The analytical accuracy of this workstation was ±11.9% in a 95% confidence interval and its corresponding absolute concentration difference was only 0.50 mM. To validate its real-world applicability, this workstation was first deployed to monitor the photoproduction of H_2O_2 over a conjugated polymer photocatalyst, DE7. In addition to performing redox titrations, we demonstrated that this workstation can also be used for acid–base titration and complexometric titration, capturing a diverse range of colour changes.

Received 18th October 2024
Accepted 26th March 2025

DOI: 10.1039/d4dd00334a

rsc.li/digitaldiscovery

Introduction

High-throughput experimental (HTE) approaches are in high demand in chemical discovery because they can free researchers from repetitive, time-intensive tasks, allowing them to dedicate more time to the creativity of chemistry.[1–3] Ideal HTE systems have low sample volume, rapid data acquisition, low cost, repeatability, modularity, and high levels of automation.[3] Recently, low-cost commercial liquid-handling robots,[4] such as Opentrons (OT-2), have been used for a variety of HTE tasks in chemistry labs. For example, Brown *et al.*[5] combined OT-2 with DESI-MS (desorption electrospray ionization mass spectrometry) to automate the reaction screening of energetic precursor cage compounds. Basford *et al.*[6] used OT-2 to accelerate the discovery process of porous organic cages, and Politi *et al.*[7] employed the OT-2 with an automated ultrasound application and a well-plate spectrometer to explore the synthesis of CdSe nanocrystals. The modularity of these platforms allowed users to customize their system based on their experimental requirements. The OT-2 platform can also be diversified by including other hardware. For example, Soh *et al.*[8] integrated a balance into the OT-2 to enable *in situ* weighing for HTE viscometry measurement of Newtonian fluids, while Ouyang *et al.*[9] installed a microscope into the OT-2 that enabled the *in situ* analysis of immunofluorescent antibody labelling.

The development of HTE approaches has benefitted from advances in computer vision.[10] For example, computer vision has aided continuous colour monitoring of chemical reactions such as pH-modulated titration experiments,[11] catalyst degradation, and product formation kinetics,[12,13] where reaction progress was linked to colour change. Furthermore, computer vision has been used for object/edge detection to assist the analysis of nanoparticles in transmission electron microscope (TEM) images[14] or cell-biomaterial analysis,[15] for solubility screening,[16,17] and for other lab automation tasks including gas flow control in organic synthesis,[18] viscosity measurement,[19] and automated real-time monitoring and control of workup processes.[20–22]

Hydrogen peroxide (H_2O_2) is one of the 100 most important chemicals due to its wide range of applications,[23,24] such as organic synthesis, paper bleaching, wastewater treatment and energy storage. In addition to the traditional commercial (but polluting) anthraquinone method,[25] researchers have investigated alternative routes such as electrocatalysis,[26,27] and

Department of Chemistry and Materials Innovation Factory, University of Liverpool, 51 Oxford Street, Liverpool, L7 3NY, UK. E-mail: c.boott@liverpool.ac.uk; aicooper@liverpool.ac.uk

† Electronic supplementary information (ESI) available. See DOI: https://doi.org/10.1039/d4dd00334a

‡ These authors contributed equally to this work.

photocatalysis.[28,29] H_2O_2 concentration can be determined by a range of characterisation methods including H_2O_2-testing strips,[30] chemical titration,[31] titration combined with optical spectroscopy,[32–34] HPLC[35] and NMR.[36] However, these methods often either suffer from low accuracy (error: ±20% for H_2O_2 tests strips), long reaction times (UV-vis and fluorimetry), or high-cost (NMR and HPLC), which may prohibit their use in HTE systems. For low-cost HTE H_2O_2 determination, colourimetric titration methods are attractive as their colour change could be easily visualised with the aid of computer vision.[37]

Here, a liquid-handling industrial robot (OT-2) was integrated with a standard webcam to enable HTE robotic titration, with H_2O_2 determination *via* $KMnO_4$ redox titration as the most detailed and well-characterized example. Unlike other hardware platforms, such as the Creality Ender 3 Pro,[38] or traditional titration setups using Arduino open-source microcontrollers,[39,40] this workstation required no prior expertise in robotics, fluid dynamics, or software development. An interactive user-friendly interface was also developed, allowing chemists without programming expertise to easily operate it. This robotic titration workstation was first utilized to monitor H_2O_2 photoproduction using an organic semiconductor photocatalyst. Furthermore, its modular design enables easy adaptation for other colourimetric titrations, including acid–base titration for acidity/alkalinity testing and complexometric titration for water hardness analysis. With the relatively low-cost and commercial availability of OT-2, this workstation is accessible for other research groups, supporting colourimetric titration endpoint analysis in their experiments and highlighting its potential for establishing an affordable, self-driven laboratory in the future.

Materials and methods

HTE H_2O_2 determination setup using OT-2

The deck layout of OT-2 for HTE H_2O_2 determination using an automated OT-2 liquid handling robot is shown in Fig. 1. The robot was equipped with one single-channel Opentrons P20 GEN2 pipette (1–20 μL) and one multi-channel Opentrons P300 GEN2 pipette (20–300 μL). Their corresponding tips were stored on deck 1, deck 8, deck 10 and deck 11, respectively. Three 12-column reservoirs (21 mL, catalogue number: 201256-100) were used to hold stock solutions, including 1 M H_2SO_4, 1 mM, 2 mM, 4 mM, and 10 mM $KMnO_4$, and testing samples, and were separately placed on deck 6, 7, and 9. One 2-column reservoir (143.87 mL, catalogue number: 203852-100) was used to store distilled water for tip rinsing. A white, flat-bottom Fisherbrand™ 96-well polystyrene plate (360 μL, catalogue number: 12-565-501) was placed in deck 5 as the reactor. The numbering rule of the samples in a 96-well plate is illustrated in Fig. 2 and the numbering rules of other labware are summarised in ESI Section 1.2.†

Correspondingly, deck 3, well number D3 was selected as the camera position and the webcam was attached to the pipette mount of OT-2. Except for the fixed position between plate and camera, the position of the remaining labware is interchangeable. Specifically, four positions (deck 4, 6, 7, and 9) were designated for liquid storage, while four positions (deck 1, 8, 10, and 11) were allocated for tips. Deck 2 remained as a spare. This flexible arrangement allows these 9 positions to be adjusted to meet the experimental demands of other titration chemistries. With the exception of the stock solution preparation, all procedures were carried out by an OT-2 liquid handling robot, controlled by a PC.

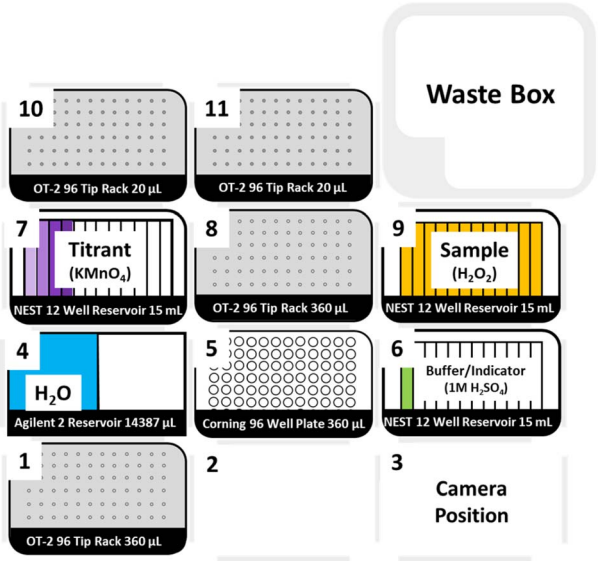

Fig. 1 The deck layout of OT-2 for HTE H_2O_2 determination using an automated liquid-handing robot OT-2 (purple = potassium permanganate solution of known concentration, $KMnO_4$; yellow = H_2O_2 samples of unknown concentration; blue = pure water; green = 1 M sulfuric acid, H_2SO_4). Deck number was placed in the upper left corner of each grid.

Workflow for automated H_2O_2 determination

The HTE H_2O_2 determination workflow can be divided into three parts: process (system configuration and transfer configuration), image capture, and signal processing (Fig. 3). The protocol development details can be found in the ESI Section 2.†

Process

System configuration. The deck number and offset of each labware and the robot configuration were defined in the system configuration (ESI Section 3†).

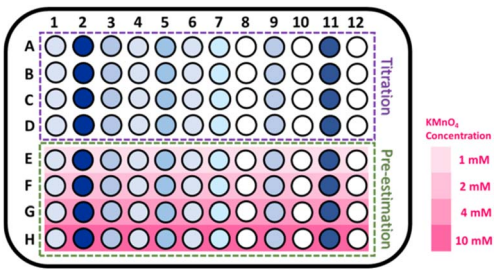

Fig. 2 Illustration of the experimental layout of a 96-well white plate. The shades of blue represent the different concentrations of H_2O_2 sample. The green area was used for pre-estimation, while the purple area was used for titration.

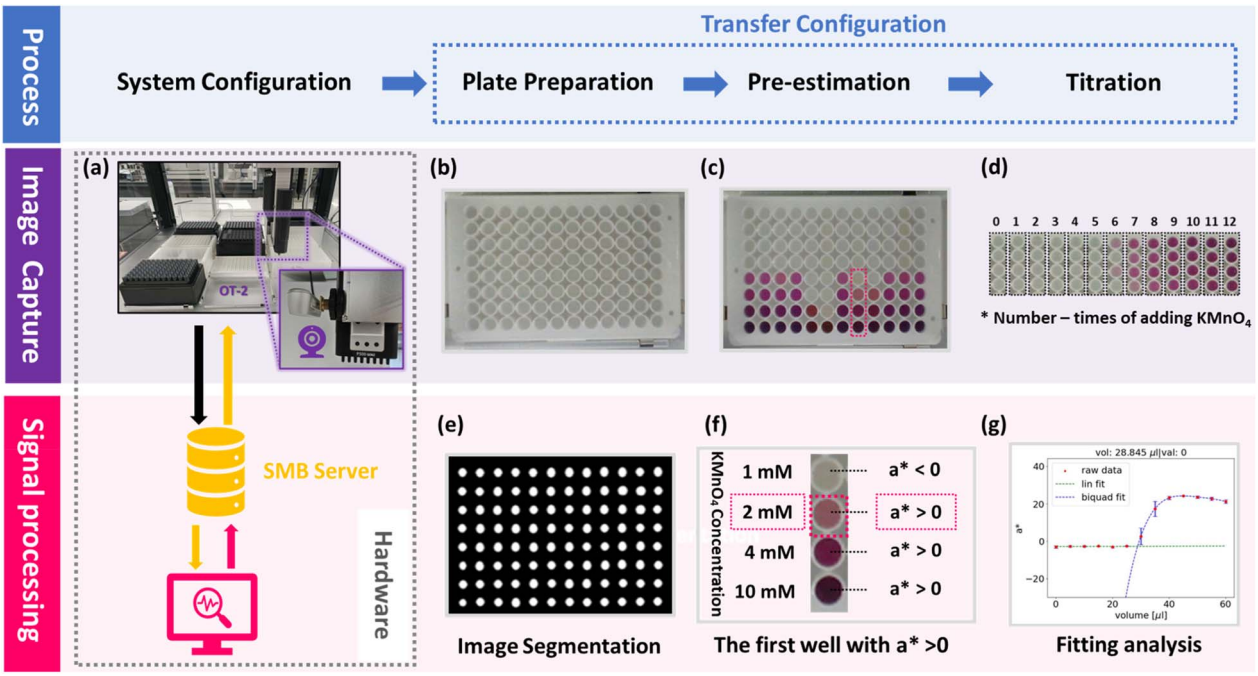

Fig. 3 Schematic representation of the HTE H_2O_2 determination workflow: (a) the illustration of the lab hardware for the HTE H_2O_2 determination and the inset image exhibited the location of the webcam on the gantry of OT-2, SMB: service message block; (b) the image of a white 96-well plate after completing the plate preparation; (c) the pre-estimation image; (d) the images captured during the titration stage; (e) the instance masks result of the plate after applying the image segmentation; (f) the illustration of the selection of $KMnO_4$ concentration in the pre-estimation stage; (g) the fitting analysis result of the titration stage.

Transfer configuration. The liquid transfers involved in this HTE H_2O_2 determination were defined in the transfer configuration for 3 steps: plate preparation, pre-estimation, and titration.

(1) Plate preparation: 100 μL, 1 M H_2SO_4 was added to the targeted columns of the plate with the multi-channel Opentrons P300 GEN2 pipette. As shown in Fig. 2, the sample to be analysed for H_2O_2 concentration was added to the eight wells in one column using the multi-channel Opentrons P300 GEN2 pipette. One plate can hold up to 12 samples.

(2) Pre-estimation: Four different $KMnO_4$ solutions (1, 2, 4 and 10 mM) were prepared and stored in the $KMnO_4$ reservoir (A1–A4) as shown in Fig. 1. 40 μL of each $KMnO_4$ solution was aspirated with the single-channel Opentrons P20 GEN2 pipette and dispensed to the rows E–H of each column sequentially, as shown in Fig. 3c and f. The calculation details of the volume of the $KMnO_4$ solution used in the pre-estimation and titration are described in Table S2.† Then, the multi-channel Opentrons P300 GEN2 pipette was used to mix the solution with a set mixing volume of 100 μL, and this step was repeated five times to obtain a homogeneous solution for analysis. Following mixing, a tip-rinsing step was added to avoid any cross contamination.

(3) Titration: 20 μL of the selected $KMnO_4$ concentration (determined in the pre-estimation step) was aspirated and then evenly dispensed in 5 μL portions to rows A–D of each column as shown in Fig. 3. Each sample was measured four times (in parallel) to minimise random error. The multi-channel Opentrons P300 GEN2 pipette was also applied to mix the solutions thoroughly. These steps were repeated 12 times for each sample.

Image capture

A webcam was installed on the pipette mount of OT-2, as shown in Fig. 3a. The camera was triggered in the plate preparation, pre-estimation, and titration to track the colour change during the titration process. Details of the webcam installation and light environment can be found in ESI Section 4.1.†

As shown in Fig. 3b, an image of the 96-well plate was captured, prior to $KMnO_4$ addition, and used as a reference for the following colour analysis. Subsequent images were then taken for the pre-estimation step (Fig. 3c) and during the titration, an image was captured after each addition of $KMnO_4$, for a total of 13 images as shown in Fig. 3d.

Signal processing

Image segmentation using VGG-augmented UNet[41] was performed on the reference image (Fig. 3b) to generate an instance mask. This mask (Fig. 3e) was then used to segment all images obtained during the experiment (for more details of the image segmentation see ESI Section 5.1†). Following this, colour information was first extracted in the RGB model and then converted to the CIELab colour space, which could provide better normalization and perceptual uniformity. Although RGB values are device-dependent, our primary focus was on monitoring colour changes over time rather than absolute colour values. Controlled lighting conditions and manual calibration

using a colour checker were implemented to ensure consistency before testing. In the CIELab colour model,[42] a^*, which represents the green-red opponent channel, was effective in quantifying colour changes in H_2O_2 titration experiment.

For the pre-estimation, the first well with $a^* > 0$ in rows E–H of the plate was identified and the corresponding $KMnO_4$ concentration of the well was used for the titration (Fig. 3f) and its analysis details could be found in ESI Section 5.2.†

For the titration, 13 points were obtained initially for each sample after signal processing. Initially, a piecewise fitting with a linear ($a^* < 0$) and a tangent ($a^* > 0$) basis function were performed (Fig. S10a and b†). This approach provided a good fitting of the results, however a decrease in a^* values was observed when $KMnO_4$ concentration was higher than 4 mM (Fig. S10c†). To minimise this effect on extracting the titration endpoint, some points were then deleted after showing a decreasing trend, but unfortunately a large deviation in titration endpoint was still obtained (Fig. S10d†). To address this, as shown in Fig. 3g, a piecewise fitting of the a^* using a linear (when $a^* < 0$) and a polynomial (when $a^* > 0$) basis function was performed. The intersection provided a volume estimate for the endpoint of the redox reaction between H_2O_2 and $KMnO_4$. This volume estimate value was further put into the designed excel (Table S4†) based on the stoichiometric relationships. For most datasets the 4th power polynomial showed good accuracy, and 3rd power polynomial was only used when there were insufficient points to perform the 4th polynomial fitting (see ESI Section 5.3† for more details).

Results and discussion

Protocol development

An automated titration protocol was developed by integrating an OT-2 robot with an image-capturing system for sample preparation, titration of H_2O_2 with $KMnO_4$ in a 96-well plate, and subsequent image capture and analysis to obtain the titration endpoint. However, performing microanalytical titration in a 96-well plate with a typical well volume of 330 μL demands careful titrant volume and concentration selections, the use of appropriate pipette assemblies, and correct setting of associated liquid transfer parameters such as mixing time, mixing volume, mixing repetition, air blowing, *etc.* Furthermore, the addition of $KMnO_4$, should also be synchronized with the imaging system such that immediately after a specific volume of $KMnO_4$ titrant is added, the imaging system is activated to accurately capture the associated colour change. Details of protocol development could be found in ESI Section 2.†

Here, we briefly describe the development of the HTE H_2O_2 determination protocol encompassing the creation of necessary instructions for the OT-2 robot, efficient service message block (SMB) communication between the local working PC and OT-2, instruction parsing and subsequent command execution by the OT-2 robot, pre-estimation method for selecting the ideal titrant, titration stage, and image capture and analysis system. Initially, an intuitive working system was built to allow OT-2 to communicate with our local working PC through an SMB server as shown in Fig. 4 (ESI Section 4.2†).

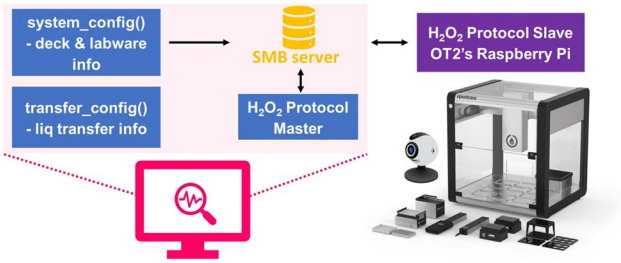

Fig. 4 The illustration of the interactive working system for HTE H_2O_2 determination (SMB server – service message block, OT-2 image reprinted with permission from Opentrons. Copyright Opentrons).

The protocol designer script, containing system configuration and transfer configuration, set the titration protocol parameters, and executing the protocol required running the master protocol and the slave H_2O_2 protocol script in tandem. The protocol designer script writes labware definition and liquid transfer instructions in the system/transfer configuration files and then stores them in the SMB server. The protocol master script was then used to initiate the execution; that is, sending a trigger signal to the slave script residing in the Raspberry Pi built into the OT-2. Upon receiving the trigger signal, Raspberry Pi positions the gantry arm to align the camera's field of view with the 96-well plate. Then, a Raspberry Pi controller sends another trigger back to the SMB server, which activates the camera that was controlled by the working PC. The images gained through these operations are also stored in the SMB server and then analysed by the computer based on the CIELab colour model through the H_2O_2 protocol master script. Following image capture, the VGG-augmented UNet[41] generates a mask (see ESI Section 5†) mapping the wells with the mask coordinates and triggers the Raspberry Pi to parse instructions from the transfer configuration.

The transfer configuration tasks were split into the following parts: plate preparation, pre-estimation, and titration. During the plate preparation stage, OT-2 transferred 1 M H_2SO_4 and H_2O_2 (concentration to be estimated) from the reservoirs defined by the system configuration (system config.) to the white 96-well plate. Our pre-estimation stage, somewhat equivalent to binning H_2O_2 by conventional stick measurements, estimated the concentration range of H_2O_2, thus aiding the selection of $KMnO_4$ titrant (range 1–10 mM) for titration (see Section 2.2). Finally, the titration stage was performed using the titrant determined by pre-estimation. Vigorous mixing of $KMnO_4$ during stepwise addition was crucial for accurately estimating the pre-estimation and titration point; otherwise, a significant phase shift of a^* *versus* $KMnO_4$ volume trace was observed. An independent mixing step was introduced to alleviate such inhomogeneity issues (for more details see ESI Section 2.3†). In this stage, 5 μL of $KMnO_4$ was sequentially added and a trigger signal was sent to the camera for image acquisition and colour extraction. This step was run until the total number of defined titration steps was exhausted (see Section 2.4). Note that the trigger signal mentioned above was just a '.csv' file containing keywords 'run' or 'done' and stored in

the SMB server. After titration, the protocol master script plotted the a^* *versus* $KMnO_4$ volume. We estimated the titration endpoint by fitting this result with piecewise continuous functions – regions with $a^* \sim 0$ and $a^* > 0$ were fitted with a linear line and an exponential, respectively.

Performance evaluation

When developing a new analytical method, there are six key figures of merit: sensitivity, precision, accuracy, linear dynamic range, detection limit, and selectivity. Here it was unnecessary to evaluate the selectivity because only the a^* parameter in CIELab colour model was monitored.

Sensitivity test and precision test. The a^* value obtained from the CIELab was compared with the absorbance value at 525 nm, the characteristic peak of $KMnO_4$, measured by a plate reader, as shown in Fig. 5.

Samples from 1 to 10 mM H_2O_2 concentration were tested for sensitivity evaluation. The H_2O_2 concentration obtained from the automated workflow based on the CIELab colour model was strongly correlated to the H_2O_2 concentration measured by the plate reader based on the UV-vis spectrometer with an R^2 of 0.9996. A slope of 0.935 and a negative intercept of −0.023 was obtained from the linear fitting, which indicated that the consumed $KMnO_4$ volume calculated from OT-2 was lower than that calculated from the plate reader. This could be attributed to the use of different types of plates. For the experiments carried out by the plate reader, a transparent 96-well plate was utilized to satisfy the light penetration requirements. While in our HTE H_2O_2 determination, a white 96-well plate was selected to achieve high contrast, which allowed the camera to observe the subtle colour change, from colourless to pale pink. This meant that a lower $KMnO_4$ volume was required for the pink colour to be detected on the OT-2 and hence a lower H_2O_2 concentration was calculated. To further verify this difference, a transparent 96-well plate was used in our workstation, and it also showed a delay to the titration endpoint (Fig. S13 and S14†).

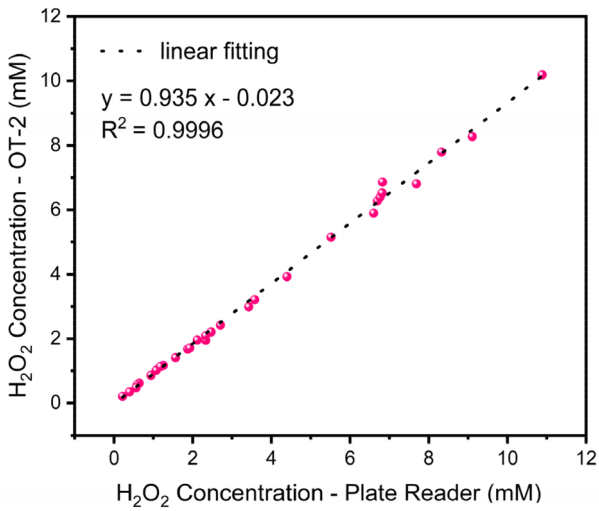

Fig. 5 Sensitivity test (x – H_2O_2 concentration determined by the plate reader, y – H_2O_2 concentration determined by the liquid robot Opentrons (OT-2)).

Table 1 The precision result of the high-throughput H_2O_2 determination using an automated pipetting robot OT-2[a]

Item	Estimated volume (μL)	Estimated conc. (mM)
Sample 1	21 ± 1	0.610 ± 0.017
Sample 2	23 ± 1	1.282 ± 0.033
Sample 3	24 ± 0	2.557 ± 0.000
Sample 4	33 ± 1	3.551 ± 0.123

[a] Note: the working limit of a single-channel P20 GEN2 pipette is 1 μL, and the $KMnO_4$ was determined by UV-vis spectrometer with three significant figures.

To estimate the reproducibility of this analytical method for H_2O_2 determination, four unknown samples of H_2O_2 concentration were randomly selected and tested three times respectively (Table 1). The low standard deviation on the estimated volume and corresponding concentration indicated that the HTE H_2O_2 determination using an automated liquid handling robot OT-2 has good repeatability. The core of our analysis method is to find the titration endpoint, a very subtle colour change from transparent to pale pink. Thus, the linear dynamic range (LDR) was also tested using a $KMnO_4$ concentration of 1 mM and it showed a good linear relevance at lower $KMnO_4$ concentrations (Fig. S15†). At higher concentrations, the colour is too saturated, which breaks down the uniformity of the CIElab colour model. However, in our case, the target is titration endpoint analysis, where the colour change is far from saturation.

Accuracy test. To evaluate the accuracy of this HTE H_2O_2 determination, the well-established iodometry method[43] (for more details see ESI Section 7.4†) was selected as the representative of true value, although it inevitably involved some human error due to the long operation times.

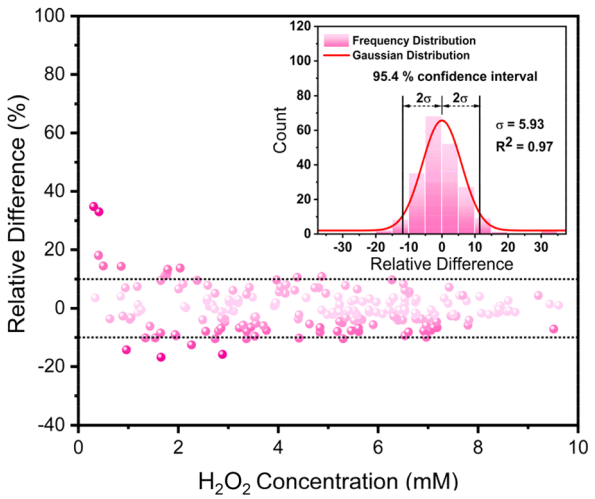

Fig. 6 The relationship between relative difference and H_2O_2 concentration (the lighter the pink dot is, the closer the relative difference is zero). The inset plot is the frequency distribution of relative difference (bin range: ±30%, bin width: 5%) and its corresponding Gaussian distribution ($x_c = 0$, $y_0 = 2$) as shown in the red line.

Over 200 random samples, with H_2O_2 concentrations between 0 and 10 mM, were prepared and tested using the automated workflow and the iodometry method (calculation details summarized in Table S6†). Fig. 6 showed that the relative difference decreased as the H_2O_2 concentration increased. This trend was also reflected by the statistical analysis, as shown in the inset plot. Within the 95.4% confidence interval, the relative difference was ±11.86%, with an R^2 of 0.97. The corresponding absolute difference was also calculated (Fig. S18†) and all deviations were lower than 1 mM (99.7% confidence interval: ±0.75 mM, 95% confidence interval: ±0.50 mM).

Operation time and scalability test. The operation time (that is, speed) is also a significant metric when evaluating the performance of an automated lab tool. For this HTE H_2O_2 determination using an automated pipetting robot OT-2, it took approximately 6 h to complete measuring 12 samples in a 96-well white plate, at around 30 minutes per sample ($n = 4$). The water evaporation rate of the $KMnO_4$ solutions was studied over time and was found to be stable over 6 h (Fig. S19†). Furthermore, the current workflow offers considerable flexibility to the user, for example, once the pre-estimation has been completed, the chemist could stop the protocol, check the results, and then just execute titration for samples of interest. In this case, the total operation time could be reduced because the operation time for the pre-estimation step is only 30 minutes. As mentioned above, efforts were made to scale down the sample testing size while capturing titration endpoint accurately. To demonstrate the flexibility of this analytical method, 24-well plates were chosen, which could allow us to explore the impact of well plate dimensions and number of wells for reaction. Due to a commercial shortage of 24-well white-coloured plates, only 24-well white plate with a clear bottom was obtained in these studies. When the titration was performed in the 24-well plate the H_2O_2 concentration (1.97 mM) determined was similar to 96-well plate concentration (H_2O_2 = 1.93 mM) (Fig. S20†). The experimental details could be found in ESI Section 7.6.†

Application. To show a real-life application, this analytical method, it was first used for monitoring a reaction with H_2O_2 as the final product. H_2O_2 photoproduction by DE7, an organic photocatalyst reported for H_2O_2 photoproduction, mostly through oxygen reduction reaction[44] was selected and its experimental details of H_2O_2 photoproduction could be seen in ESI Section 8.1.† As shown in Fig. 7, the H_2O_2 photoproduction over time as catalysed by DE7 was accurately monitored by our HTE H_2O_2 determination, and the absolute difference between the OT-2 workstation and the iodometry method was low and became smaller with the increase in H_2O_2 concentration.

To highlight the modularity feature of this designed workstation, some other titration chemistries were also tested on our platform. Initially, colour parameters (L, a^*, b^*, R, G, B, C, h) were evaluated as a preparatory step for other applications. Among these, the hue parameter from the CIELCh colour model, a model that directly derives its scale values from CIE-Lab colour model, was selected for its ability to distinguish different colours while being less affected by solution concentration (Fig. S21†). More details on parameter selection could be found in ESI Section 8.2.† Subsequently, we modified the code,

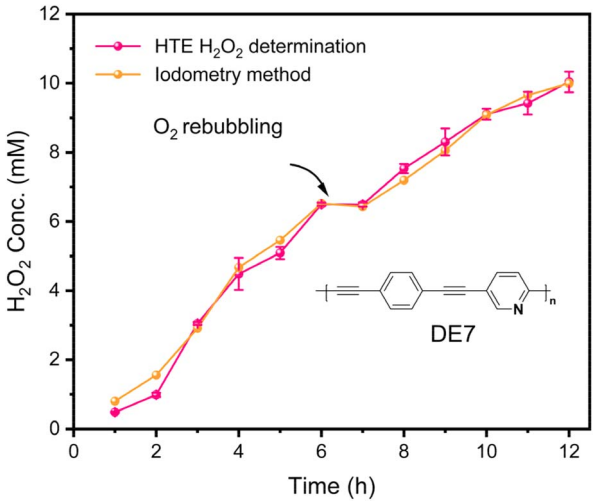

Fig. 7 The H_2O_2 photoproduction over photocatalyst DE7. The error bar is the standard deviation of HTE H_2O_2 determination, where each sample was measured four times in parallel.

to make the user interface easier for chemists navigate and use with their selected titration chemistry. This flexibility expands the operational space for chemists, enhancing the universality of the workstation.

To demonstrate the ability of this workstation to analyse diverse titration chemistries and hence capture different colour changes, the acidity/alkalinity test and water hardness analysis were selected as proof-of-concept systems. The acidity/alkalinity test, critical for ensuring quality in the food,[45] beverage,[46] or cosmetics industry,[47] were assessed *via* titration using methyl orange as the pH indicator (ESI Section 8.3†). For this titration, the colour shifts from red to yellow, corresponding to a hue shift from ~30 to ~60 (Fig. S22†). Another example is water hardness analysis (calcium ions (Ca^{2+}) analysis by ethylenediaminetetraacetic acid disodium salt dihydrate (EDTA) titration),[48,49] a typical complexometric titration. Proper identification and management of water hardness could help individuals and industries reduce costs, improve equipment efficiency, safeguard health, and maintain ecological balance. During titration, Ca^{2+} was chelated by EDTA at pH = 10, employing Eriochrome Black T as an indicator, producing a colour shift from wine red to purple and finally blue, with a corresponding hue transition from ~350 to ~220 (Fig. S23†). For both titrations, our workstation was able to effectively capture the titration endpoint using the hue parameter. This demonstrates that by appropriate colour parameter selection this workstation can monitor a broad range of colourimetric titrations (for more details see ESI Section 8.4†). The code details on the development of these two new applications, to assist in transferring this workstation to a new application, can be found here: **https://github.com/yuanlee0325/HTE-robotic-titration-using-computer-vision.git**

Limitation. While this workstation, with the integration of a liquid handling robot (OT-2) and a webcam fixed on the pipette mount of OT-2, has already achieved titration endpoint analysis accurately, it still has some limitations.

First, the system is designed for aqueous samples that exhibit distinct colour changes at the titration endpoint, facilitating precise colour analysis. However, challenges may arise when analysing opaque samples or highly saturated colours. Additionally, the current fitting analysis for the titration does not incorporate advanced algorithms to optimize the selection of fitting functions. If it could correlate colour to reagent concentration, this would unlock greater analytical potential of our designed workstation in chemistry. Finally, when performing more complex chemistries on the workstation, certain limitations may arise, including restricted deck space, non-inert atmosphere, and the requirement that all reagents must be in liquid or solution form.

Conclusion

A HTE robotic colourimetric titration workstation was established using a commercially available liquid handling robot, OT-2, equipped with a webcam. This innovative workstation facilitates *in situ*, automated, and low-cost H_2O_2 determination through the application of computer vision. In comparison with the traditional $KMnO_4$ titration, only microlitres of sample volume were required in this proposed analytical method, significantly reducing sample volume. Furthermore, the pre-estimation step provides considerable flexibility, enabling chemists to selectively perform titrations only on samples of interest. For instance, titration could be limited to catalysts exceeding a specific hydrogen peroxide production threshold, thus saving time and resources. Beyond H_2O_2 determination, this workstation exhibited applicability across various titration-based analyses, involving colour change. For example, our workstation has already successfully performed the three main titration types: redox titration, acid–base titration, and complexometric titration.

The modular design of this workstation also confers extensive adaptability, presenting opportunities to construct low-cost, self-driven laboratories. Initially, through modifications to the computer vision approach, this workstation could also achieve object/edge detection, which is a powerful tool for automated materials chemistry (*e.g.*, to locate crystals or particles). This workstation could be further extended to the integration with other digital laboratory tools to support comprehensive workflows for materials discovery in self-driven lab. For example, it could serve as an H_2O_2 quantitation tool within our existing photocatalytic workflow,[50] thereby expediting the development of photocatalysts. Or, it could be coupled with flow chemistry setups to monitor reaction progress, such as dye degradation, where yield correlates with observable colour change. Collectively, these features underscore the potential of this workstation as a tool for advancing automation and efficiency in chemical search.

Data availability

The code for 'High-throughput Robotic Colourimetric Titration Using Computer Vision' is available at **https://doi.org/10.5281/zenodo.14895187**. The specific version employed in this study is v2. Additionally, the corresponding repository for this work can be accessed at **https://github.com/yuanlee0325/HTE-robotic-titration-using-computer-vision.git**. A video demonstrating the fully automated process of high-throughput robotic determination of hydrogen peroxide (H_2O_2), integrating a liquid handling robot (Opentrons, OT-2) with a standard webcam based on chemical titration, is available at **https://doi.org/10.5281/zenodo.13825238**. Except for the basic electronic ESI,† other analysis scripts and datasets supporting this article are included in a Data.zip folder: (1) redox titration between H_2O_2 and potassium permanganate ($KMnO_4$), (2) acid–base titration using methyl orange as a pH indicator, (3) complexometric titration for Ca^{2+} analysis, and (4) scalability test. This folder is also accessible at **https://doi.org/10.5281/zenodo.14895187**.

Author contributions

C. E. B. and A. I. C. devised and supervised the project. Y. L. carried out all experiments and led the experimental work. Y. L. and B. D. designed the protocol. B. D. wrote the script to control the system and Y. L. modified the code to enhance its adaptability for various titration chemistries. Q. J. Y. assisted with the fitting model optimization for data analysis. B. D. and R. C. assisted with the hardware construction and R. C. helped with the photocatalytic H_2O_2 production experiments. Y. L., B. D., C. E. B., and A. I. C. wrote the manuscript with input from all authors.

Conflicts of interest

There are no conflicts to declare.

Acknowledgements

Y. L. acknowledges the financial support from China Scholarship Council (CSC). B. D. received funding from the Cleaner Futures Prosperity Partnership (Next-Generation Sustainable Materials for Consumer Products) funded by the Engineering and Physical Sciences Research Council (EPSRC: grant EP/V038117/1). Q. J. Y. received funding from the Engineering and Physical Sciences Research Council (EPSRC: grant EP/V026887/1). A. I. C. thanks the Royal Society for a Research Professorship (RSRP\S2\232003). The authors thank Hang Qu for discussion on data analysis, and all the reviewers for much-valued comments.

References

1 A. Slattery, Z. Wen, P. Tenblad, J. Sanjosé-Orduna, D. Pintossi, T. Den Hartog and T. Noël, *Science*, 2024, **383**, 1–12.
2 W. Zhao, P. Yan, B. Li, M. Bahri, L. Liu, X. Zhou, R. Clowes, N. D. Browning, Y. Wu, J. W. Ward and A. I. Cooper, *J. Am. Chem. Soc.*, 2022, **144**, 9902–9909.
3 T. J. P. Sobreira, L. Avramova, B. Szilagyi, D. L. Logsdon, B. P. Loren, Z. Jaman, R. T. Hilger, R. S. Hosler, C. R. Ferreira, A. Koswara, D. H. Thompson, R. G. Cooks and Z. K. Nagy, *Anal. Methods*, 2020, **12**, 3654–3669.

4 S. Lo, S. G. Baird, J. Schrier, B. Blaiszik, N. Carson, I. Foster, A. Aguilar-Granda, S. V Kalinin, B. Maruyama, M. Politi, H. Tran, T. D. Sparks and A. Aspuru-Guzik, *Digital Discovery*, 2024, **3**, 842–868.
5 H. M. Brown and P. W. Fedick, *React. Chem. Eng.*, 2023, **8**, 556–562.
6 A. R. Basford, S. K. Bennett, M. Xiao, L. Turcani, J. Allen, K. E. Jelfs and R. L. Greenaway, *Chem. Sci.*, 2024, **15**, 6331–6348.
7 M. Politi, F. Baum, K. Vaddi, E. Antonio, J. Vasquez, B. P. Bishop, N. Peek, V. C. Holmberg and L. D. Pozzo, *Digital Discovery*, 2023, **2**, 1042–1057.
8 B. W. Soh, A. Chitre, W. Y. Lee, D. Bash, J. N. Kumar and K. Hippalgaonkar, *Digital Discovery*, 2023, **2**, 481–488.
9 W. Ouyang, R. W. Bowman, H. Wang, K. E. Bumke, J. T. Collins, O. Spjuth, J. Carreras-Puigvert and B. Diederich, *Adv. Biol.*, 2022, **6**, 2101063.
10 G. Bradski, The Opencv Library, *Dr. Dobb's J.*, 2000, **25**, 120–125.
11 Y. Kosenkov and D. Kosenkov, *J. Chem. Educ.*, 2021, **98**, 4067–4073.
12 C. Yan, M. Cowie, C. Howcutt, K. M. P. Wheelhouse, N. S. Hodnett, M. Kollie, M. Gildea, M. H. Goodfellow and M. Reid, *Chem. Sci.*, 2023, **14**, 5323–5331.
13 H. Barrington, T. J. D. McCabe, K. Donnachie, C. Fyfe, A. McFall, M. Gladkikh, J. McGuire, C. Yan and M. Reid, *Angew. Chem., Int. Ed.*, 2025, **64**, e202413395.
14 X. Wang, J. Li, H. D. Ha, J. C. Dahl, J. C. Ondry, I. Moreno-Hernandez, T. Head-Gordon and A. P. Alivisatos, *J. Am. Chem. Soc. Au*, 2021, **1**, 316–327.
15 R. Owen, A. Nasir, M. H. Amer, C. Nie, X. Xue, L. Burroughs, C. Denning, R. D. Wildman, F. A. Khan, M. R. Alexander and F. R. A. J. Rose, *Adv. Intell. Syst.*, 2024, 2400573.
16 P. Shiri, V. Lai, T. Zepel, D. Griffin, J. Reifman, S. Clark, S. Grunert, L. P. E. Yunker, S. Steiner, H. Situ, F. Yang, P. L. Prieto and J. E. Hein, *iScience*, 2021, **24**, 102176.
17 G. Pizzuto, J. De Berardinis, L. Longley, H. Fakhruldeen and A. I. Cooper, in *Proceedings of the International Joint Conference on Neural Networks*, Institute of Electrical and Electronics Engineers Inc., 2022, vol. 2022, pp. 1–7.
18 S. V. Ley, R. J. Ingham, M. O'brien and D. L. Browne, *Beilstein J. Org. Chem.*, 2013, **9**, 1051–1072.
19 M. Walker, G. Pizzuto, H. Fakhruldeen and A. I. Cooper, *Digital Discovery*, 2023, **2**, 1540–1547.
20 R. El-khawaldeh, A. Mandal, N. Yoshikawa, W. Zhang, R. Corkery, P. Prieto, A. Aspuru-Guzik, K. Darvish and J. E. Hein, *Device*, 2024, 100404.
21 R. El-Khawaldeh, M. Guy, F. Bork, N. Taherimakhsousi, K. N. Jones, J. M. Hawkins, L. Han, R. P. Pritchard, B. A. Cole, S. Monfette and J. E. Hein, *Chem. Sci.*, 2024, **15**, 1271–1282.
22 A. E. Siemenn, E. Aissi, F. Sheng, A. Tiihonen, H. Kavak, B. Das and T. Buonassisi, *Nat. Commun.*, 2024, **151**, 1–11.
23 H. Hou, X. Zeng and X. Zhang, *Angew. Chem., Int. Ed.*, 2020, **59**, 17356–17376.
24 F. Y. Yu, Y. J. Zhou, H. Q. Tan, Y. G. Li and Z. H. Kang, *Adv. Energy Mater.*, 2023, 2300119.
25 J. M. Campos-Martin, G. Blanco-Brieva and J. L. G. Fierro, *Angew. Chem., Int. Ed.*, 2006, **45**, 6962–6984.
26 C. Xia, Y. Xia, P. Zhu, L. Fan and H. Wang, *Science*, 2019, **366**, 226–231.
27 S. R. Kelly, X. Shi, S. Back, L. Vallez, S. Y. Park, S. Siahrostami, X. Zheng and J. K. Nørskov, *ACS Catal.*, 2019, **9**, 4593–4599.
28 Y. Zhang, C. Pan, G. Bian, J. Xu, Y. Dong, Y. Zhang, Y. Lou, W. Liu and Y. Zhu, *Nat. Energy*, 2023, **8**, 361–371.
29 H. Tan, P. Zhou, M. Liu, Q. Zhang, F. Liu, H. Guo, Y. Zhou, Y. Chen, L. Zeng, L. Gu, Z. Zheng, M. Tong and S. Guo, *Nat. Synth.*, 2023, **2**, 557–563.
30 Z. Lu, G. Chen, S. Siahrostami, Z. Chen, K. Liu, J. Xie, L. Liao, T. Wu, Di. Lin, Y. Liu, T. F. Jaramillo, J. K. Nørskov and Y. Cui, *Nat. Catal.*, 2018, **1**, 156–162.
31 Y. Shiraishi, S. Kanazawa, Y. Sugano, D. Tsukamoto, H. Sakamoto, S. Ichikawa and T. Hirai, *ACS Catal.*, 2014, **4**, 774–780.
32 Z. Wei, M. Liu, Z. Zhang, W. Yao, H. Tan and Y. Zhu, *Energy Environ. Sci.*, 2018, **11**, 2581–2589.
33 L. Liu, M. Y. Gao, H. Yang, X. Wang, X. Li and A. I. Cooper, *J. Am. Chem. Soc.*, 2021, **143**, 19287–19293.
34 B. O. Burek, D. W. Bahnemann and J. Z. Bloh, *ACS Catal.*, 2019, **9**, 25–37.
35 U. Pinkernell, S. Effkemann and U. Karst, *Anal. Chem.*, 1997, **69**, 3623–3627.
36 Y. B. Monakhova and B. W. K. Diehl, *Anal. Methods*, 2016, **8**, 4632–4639.
37 L. F. Capitán-Vallvey, N. López-Ruiz, A. Martínez-Olmos, M. M. Erenas and A. J. Palma, *Anal. Chim. Acta*, 2015, **899**, 23–56.
38 A. Kopyl, Y. Yew, J. Wern Ong, T. Hiscox, C. Young, M. Muradoglu and T. Wah Ng, *J. Chem. Educ.*, 2024, **101**, 640–646.
39 R. Soong, K. Agmata, T. Doyle, A. Jenne, A. Adamo and A. J. Simpson, *J. Chem. Educ.*, 2019, **96**, 1497–1501.
40 K. S. Tay and J. L. Eng, *J. Chem. Educ.*, 2024, **101**, 5430–5436.
41 V. Iglovikov and A. Shvets, *arXiv*, 2018, preprint, arXiv:1801.05746, DOI: **10.48550/arXiv.1801.05746**.
42 N. Phuangsaijai, J. Jakmunee and S. Kittiwachana, *J. Anal. Sci. Technol.*, 2021, **12**, 1–16.
43 P. Garcia-Munoz, L. Valenzuela, D. Wegstein, T. Schanz, G. E. Lopez, A. M. Ruppert, H. Remita, J. Z. Bloh and N. Keller, *Top. Curr. Chem.*, 2023, **381**, 1–73.
44 L. Liu, M. Y. Gao, H. Yang, X. Wang, X. Li and A. I. Cooper, *J. Am. Chem. Soc.*, 2021, **143**, 19287–19293.
45 D. D. Miller and C. K. Yeung, *Food Chemistry: A Laboratory Manual*, Wiley, Hoboken, 2nd edn, 2022, p. 199.
46 W. K. Tan, Z. Husin, M. L. Yasruddin and M. A. H. Ismail, *J. Food Sci. Technol.*, 2023, **60**, 1681–1694.
47 M. Lukić, I. Pantelić and S. D. Savić, *Cosmet*, 2021, **8**, 69.
48 S. S. Nielsen, *Food Analysis Laboratory Manual*, ed. S. S. Nielsen, Springer, Cham, 2017, ch. 16, pp. 147–152.
49 D. Damasceno, T. G. Toledo, A. Da Silva Soares, S. Botelho De Oliveira and A. Elcana De Oliveira, *Anal. Methods*, 2016, **8**, 7832–7836.
50 B. Burger, P. M. Maffettone, V. V. Gusev, C. M. Aitchison, Y. Bai, X. Wang, X. Li, B. M. Alston, B. Li, R. Clowes, N. Rankin, B. Harris, R. S. Sprick and A. I. Cooper, *Nature*, 2020, **583**, 237–241.